# We are IntechOpen,
# the world's leading publisher of Open Access books
# Built by scientists, for scientists

**4,800**
Open access books available

**122,000**
International authors and editors

**135M**
Downloads

**154**
Countries delivered to

Our authors are among the

**TOP 1%**
most cited scientists

**12.2%**
Contributors from top 500 universities

WEB OF SCIENCE™

Selection of our books indexed in the Book Citation Index
in Web of Science™ Core Collection (BKCI)

Interested in publishing with us?
Contact book.department@intechopen.com

Numbers displayed above are based on latest data collected.
For more information visit www.intechopen.com

# Central Changes in Glaucoma: Neuroscientific Study Using Animal Models

Kazuyuki Imamura et al.*
*Dept. Systems Life Engineering, Maebashi Institute of Technology, Maebashi-shi, Japan*

## 1. Introduction

The relatively high incidence of glaucoma has become a serious health problem in the rapidly aging society (Elolia and Stokes, 1998; Klein et al., 1992; Leske, 1983; Salive et al., 1992 ). Adequate animal models are thus urgently needed to develop an effective remedy(s) of glaucoma or even to prevent its occurence. Death of retinal ganglion cells (RGC) death is the major pathological feature of glaucoma, and has been studied extensively at the level of the retina focused on the optic nerve head. Visual field deficit caused by the loss of RGCs in glaucoma must be accompanied by morphological and physiological changes in the higher visual centers. However, limited knowledge is available concerning the trans-synaptic changes, in morphology and physiology, induced in the central visual system by glaucoma.

Our basic premise is that the centripetal changes in glaucoma may precede those in the eye, because compensation processes for the deteriorating function are, in general, much fast or strongly expressed in the central system than peripheral system due to the increased level of complexity in the former. Provided that this is the case, the detection of central changes is critical for establishing the early diagnosis of glaucoma in its initial stage.

The number of photoreceptors in the retina is about one billion, while that of optic nerve fibers is about one hundred and twenty million. By a simple calculation, therefore, it is likely that there is substantial afferent convergence or integration within neural network of the retina before visual output sent out along the centripetal pathway. Thus, abnormal retinal outputs in glaucoma to the lateral geniculate nucleus (LGN) are thought to induce compensatory responses in thalamic and visuocortical neurons. We would like to examine such changes in morphology and physiology as a harbinger of glaucomatous changes in visual function.

*Masamitsu Shimazawa[1], Hirotaka Onoe[2], Yasuyoshi Watanabe[2], Kiyoshi Ishii[3], Chihiro Mayama[3], Takafumi Akasaki[4], Satoshi Shimegi[5], Hiromichi Sato[5], Kazuhiko Nakadate[6], Hideaki Hara[1] and Makoto Araie[4]

[1]Molecular Pharmacology, Dept. Biofunctional Evaluation, Gifu Pharmaceutical Univ., Gifu-shi, Gifu 501-1196, Japan
[2]RIKEN Center for Molecular Imaging Science, Japan
[3]Dept. Ophthalmology, Graduate School of Medicine and Faculty of Medicine, Univ. of Tokyo, Japan
[4]Dept. Intelligent System, Faculty of Computer Science and Engineering, Kyoto Sangyo University, Kyoto-shi, Japan
[5]Lab. Cognitive and Behavioral Neuroscience, Graduate School of Medicine, Osaka University, Toyonaka-shi, Japan
[6]Dept. Histology and Neurobiology, Graduate School of Medicine, Dokkyo Medical University, Japan

A monkey model of unilateral hypertension glaucoma has been successfully created by laser irradiation to the trabecular meshwork: experimental monkeys exhibited, when ophthalmologically examined, sustained and reproducible increase in intraocular pressure (IOP) for a relatively long period (Shimazawa et al., 2006a, b). Lately, experimentally induced changes in the primary visual pathway were reported findings by ophthalmological examinations of monkeys studied by using PET in monkeys with unilateral hepertension glaucoma. In addition, the time course of changes in appearance of the optic disk and thickness of the retinal nerve fiber layer (RNFL) measured by scanning laser ophthalmoscopy (HRT) and scanning laser polarimetry (GDx), exhibited corresponding changes in hypertension glaucoma of human. The latter measurement was in good correlations with RNFL thickness determined histologically (Shimazawa et al., 2006b). Visual field loss in glaucomatous monkeys was also studied by a behavioral method (Sasaoka et al., 2005).

In this chapter, we describe a set of new findings we obtained for the centripetal changes in hypertension glaucoma, which is experimentally induced by unilateral laser coagulation of the trabeclar meshwork of monkeys. Data-analysis methods employed here include: imaging with positoron emission tomography (PET), neuroanatomical tracing, immunohistochemical staining, and electrophysiological single-unit recording.

## 2. Two new findings in glaucomatous monkeys obtained by PET

PET is a powerful, noninvasive imaging technology widely used in examination of brain function (Giovacchini et al., 2011). As reported previously (Imamura et al., 2009), we found in a PET study with 2-[$^{18}$F]fluoro-2-deoxy-glucose on glaucomatous monkeys that monocular visual stimulation of the affected eye yielded significantly reduced neural responses in the occipital areas of visual cortices. Intriguingly, the reduction in response was limited to the cortex ipsilateral to the affected eye, indicating the unique vulnerability of ipsilateral visual cortex in glaucomatous monkeys (Imamura et al., 2009).
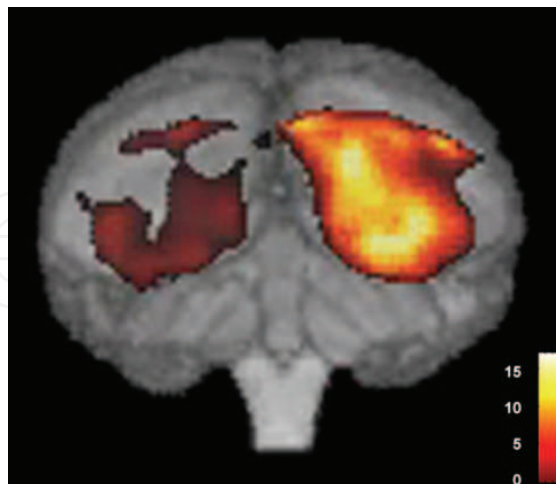


Fig. 1. A symmetric activation of occipital cortex in glaucomatous monkey. Modified from NeuroReport, (Imamura et al., 2009)

Characteristic pattern of $^{18}$FDG uptake during monocular activation is shown as a back view of monkey brain. Statistical parametric mapping (SPM) analysis was performed using six images obtained form two model monkeys. The results of SPM analysis (t-values), with data from six

PET images for each eye of two monkeys, are superimposed on the T1 image of one monkey. The color scale indicated the t-value, the level of significance (P<0.05, red to P<0.00001, white). Note that left visual cortex ipsilateral to the affected eye exhibited significantly lower activity, suggesting deterioration of function in the ipisilateral visual pathway.

Next, using [$^{11}$C]PK11195, a PET tracer for peripheral benzodiazepine receptors, we found selective binding in the LGN of glaucomatous monkeys, while no binding was found in other brain regions. In the central nervous system, the expression of peripheral benzodiazepine receptors are limited to the activated microglia, which in turn exhibits neurotoxic, neurotrophic and neuroprotective activities by releasing several types of cytokines, including NO, TNF-$\alpha$, and IL-1ß. The binding of [$^{11}$C]PK11195 was earlier reported only in the diseased brain, for example, in multiple sclerosis (Vowinckel et al., 1997), herpes encephalitis (Cagnin, et al., 2001b), and Alzheimer disease (Cagnin, et al., 2001a). In short, the present finding indicates that, in our model monkeys, hypertension glaucoma induces the activation of the microglia in the LGN suggestive of some functional changes in the LGN.
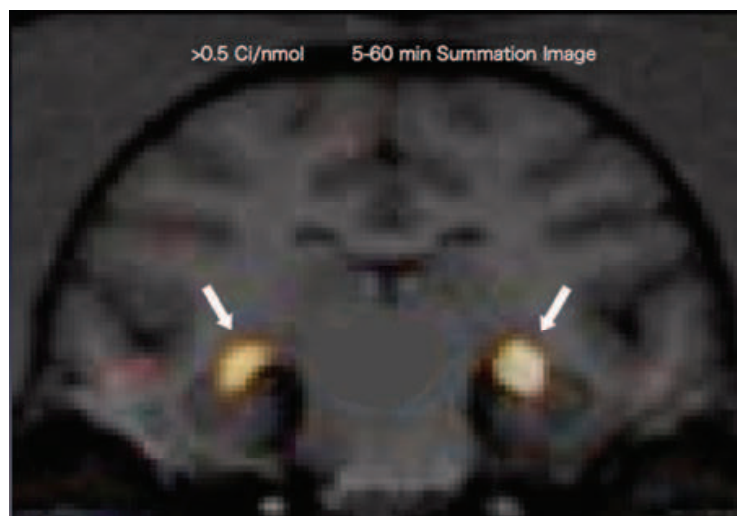


Fig. 2. Accumulation of [$^{11}$C]PK11195 activity in the LGN. A PET summation image is superimposed on an MRI T1 image. The PET image in the frontal plane shows selective accumulation of activity in the LGN of both hemispheres (arrows). Modified from NeuroReport, (Imamura et al., 2009)
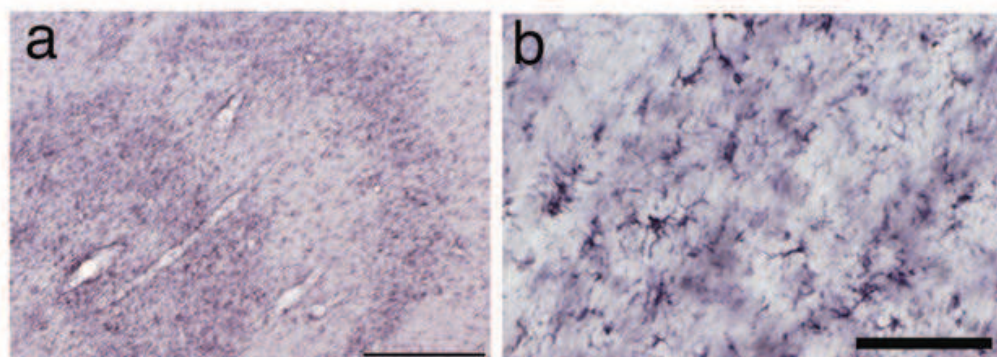


Fig. 3. Immunohistochemical staining of activated microglia in the LGN of glaucomatous monkey. Higher power view of a stained layer is shown (b). Scale bars show 500 µm (a) and 200 µm (b), respectively.

To clarify the above point, we further performed an immunohistochemical study using specific antibody against activated microglia (Graeber et al., 1994). Results indicated that the immunoreactivity was confined indeed to the LGN layers that normally receive afferent inputs from the glaucoma-affected eye. The termination pattern of retinal axons in the LGN is known to eye-selective, with one layer receiving input only from one eye. Accordingly, the staining pattern we found was complimentary between the left and right and left LGNs. Immunohistochemical staining was performed using CR3/43 antibody, which selectively recognizes activated microglia. Laminar selective staining (a) was found. The stained layers were found to receive inputs from the glaucomatous eye.

## 3. Selective damage of centripetal visual pathway ipsilateral to affected eye

Next we asked why the activity in the visual cortex was selectively reduced in the hemisphere ipsilateral to the affected eye. We performed neuroanatomical tracing experiments using wheat germ agglutinin (WGA) as an anterograde tracer. WGA was injected into normal eye of naive monkeys and both normal and affected eyes of the glaucomatous monkeys. After a survival period of 3 days for anterograde transport of the tracer, the animals were perfused with 4 % paraformaldehyde, the brain was removed and immunohistochemical staining of thin LGN section was performed using an anti-WGA antibody (Gong & LeDoux, 2003).

First, in the case of the normal eye of a naive monkey, individual layers of the LGN that receive input from the injected eye were stained (Fig. 4). At higher magnification (Fig. 5), it was clearly seen that postsynaptic neurons were transsynaptically labeled with some granular staining pattern that reflected endings of the afferent nerve fibers (Fig. 5).
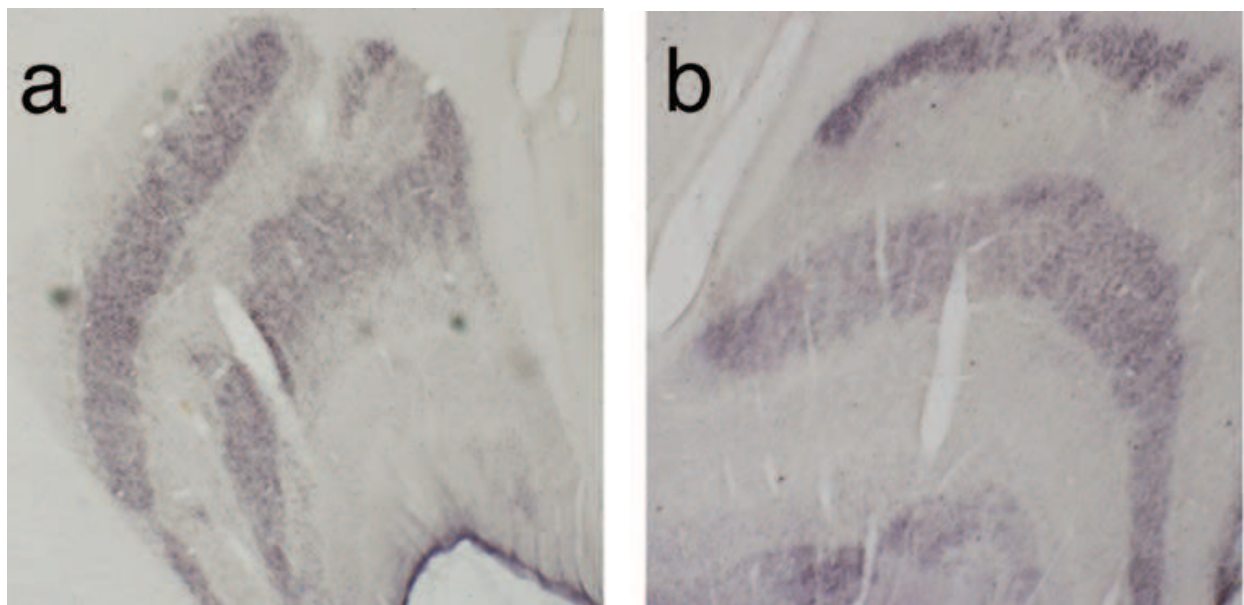


Fig. 4. Immunohistochemical staining of normal LGN, using anti-WGA antibody after monocular injection of WGA In the case of naive animal, the left (a) and right (b) LGN exhibit complementary staining pattern of layers that receive afferents from the injected eye. Scale, 1 mm.
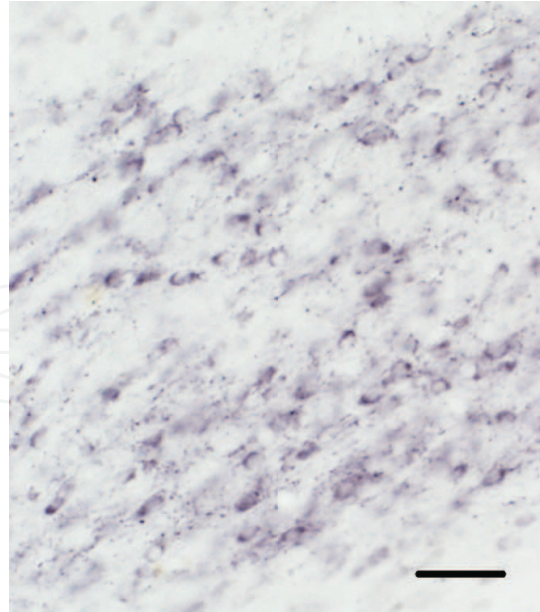
Fig. 5. Transsynaptic transport of WGA in the LGN. Labeling of postsynaptic neurons was found in the form of granular, presumably presynaptic, staining in a layer of the LGN. Scale, 50 μm.

Figure 6 shows the results of a case, in which the tracer was injected into the normal eye of glaucomatous monkey. A complementary staining pattern similar to that found with the aforementioned case was obtained. In addition, discordant staining was sometimes found invading into neighboring layers that should be free of the input from the injected eye. Finally, a tracer injection was performed into the affected eye of the glaucomatous monkey. In one of the two monkeys examined, no transport of WGA was found in the LGN, while in the other animal selective staining was found only in the input-receiving layers of the LGN contralateral to the injected eye. No staining was found in the ipsilateral LGN (Fig. 7).
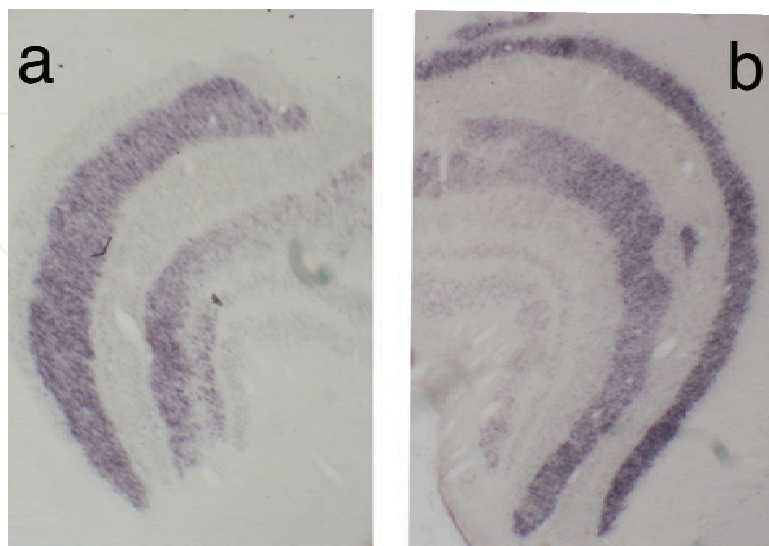


Fig. 6. Staining pattern of the left (a) and right (b) LGN of glaucomatous monkey when WGA was injected into the fellow eye. Scale, 1 mm.
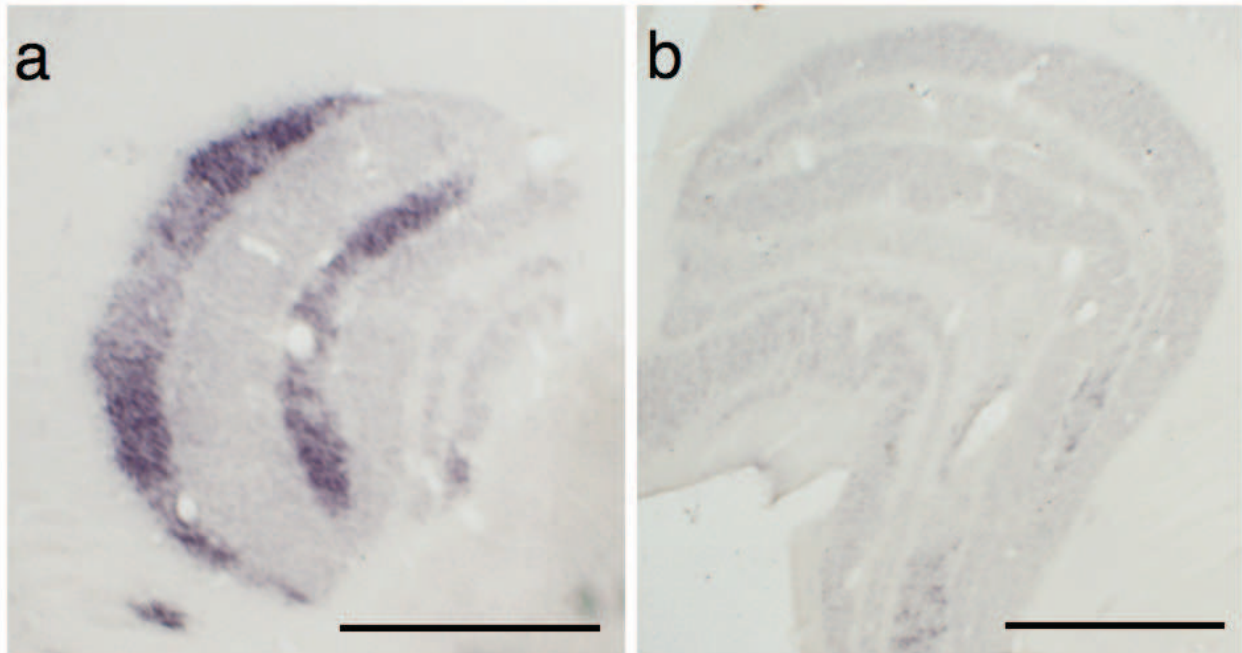
Fig. 7. Staining pattern of the left (a) and right (b) LGN of glacomatous monkey when WGA was injected into the affected eye.  Scale, 1 mm.

In the right LGN, the staining was found in layers 6 and 4 and a part of 1, all of which usually receive input from the injected eye.  In the left LGN ipsilateral to the glaucomatous eye, some faint staining was seen in the ventrolateral parts of layers 5 and 3.  These results indicate that the normal retinal projection to the LGN was reserved only for in the contralateral pathway, strongly suggesting that the ipsilateral pathway was vulnerable to the elevation of IOP.  This asymmetry indicated that injury of retinal ganglion cells in the temporal retina was more severe than that in the nasal retina.  Interestingly, reduction of nasal-temporal asymmetry was reported in normal-tension glaucoma (Asano et al., 2007). Likewise, in strabismic amblyopes, reduced monocular activation was selectively detected only in visual cortex ipsilateral to the deprived eye (Imamura et al., 1997).  Taken together, the present result suggest the high vulnerability of the ipsilateral projection in these patho-physiological conditions.

Electronmicroscopic examinations revealed that the optic nerve fibers derived from the glaucomatous eye were shrunken and damaged. In particular, the outer part was damaged more severely than the central part of the nerve trunk (Fig. 8).  It was reported that in humans, optic nerve axons are not instructed to establish a retinotopic order within the initial portion of the visual pathway (Fitzgibbon and Taylor, 1996).  However, in our model monkeys, vulnerability of the outer part of the optic nerve is frequently found.

## 4. Mechanisms of the induction of activated microglia in the LGN of glaucomatous animals

To obtain clues for the activation of the microglia in the LGN of glaucomatous monkeys, the following experiments were performed in the mouse LGN.  First, we suspected that the microglia in the LGN was activated as a consequence of the substantial reduction of neural activity in the retina of the glaucomatous monkeys. Then, under isoflurane anesthesia, one eye of the mouse was injected with either tetrodotoxin (TTX), a sodium channel blocker, or
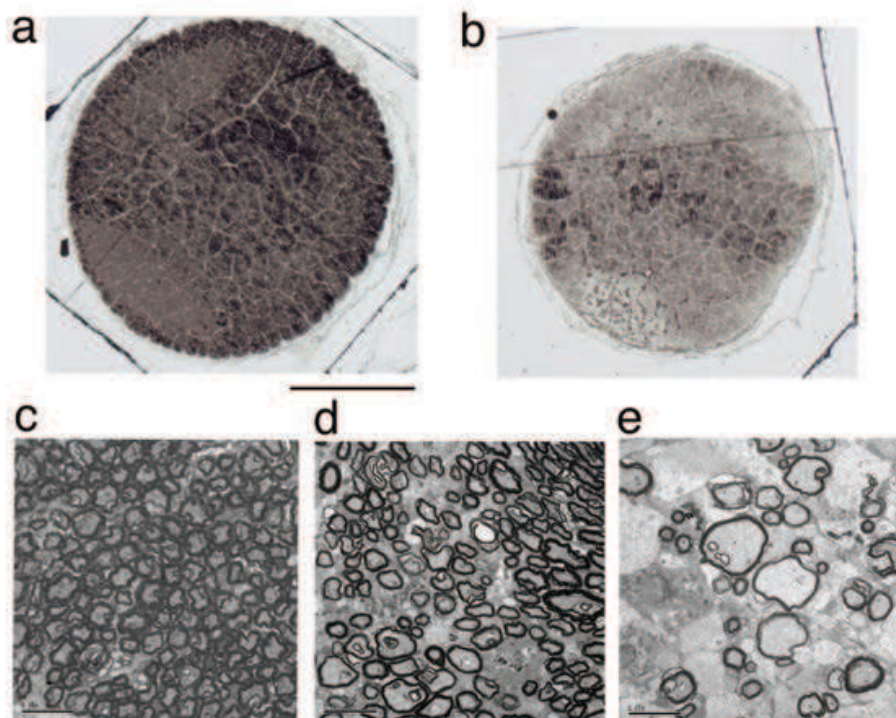
Fig. 8. Electronmicroscopic view of the optic nerve.
In lower-power view, it is clear that the optic nerve derived from the glaucomatous eye (b) is profoundly damaged when compared with that from the fellow eye (a). Scale, 1mm. In the high-power view, severe demyelination was observed in the outer part of the optic nerve (e), while the central dark portion exhibit a trace of myelinated fibers (d). However, the density of myelinated fibers was reduced in (d) and (e) compared with the optic nerve from the fellow eye (c).

N-methyl-D aspartate (NMDA), an agonist of NMDA-type glutamatergic receptors to suppress neuronal electrical activity or enhance excitability of retinal cells, respectively. One week after the respective eye injection, animals were perfused and immunohistochemical analysis was performed using antibodies to zif268 protein, a neuronal activity marker, and ionized calcium binding adaptor molecules 1 (Iba 1), a marker of microglia. In mice, the superior colliculus (SC) is the major recipient site of the retinal afferents. As expected, an asymmetrical staining pattern of Zif268 was seen in the SC of the mice monocularly injected with TTX (Fig. 9), while little difference was found in the SC of NMDA-injected mice (not shown). Rather, a slight enhancement was found in the SC contralateral to the NMDA-injected eye.

These results showed that each of the two chemical injected into one eye affected retinal neuronal activities in an expected manner. In the LGN of these mice, for sure, the activated microglias were induced following the TTX injection, although their number was small when compared with that following monocular enucleation, a measure that is much stronger than the former (Fig. 10). Taken together, these findings suggested that when the retinal activity was substantially outside of a certain range, activated microglia were induced in the LGN.

In our monkey model, the retinal activity was clearly suppressed in the IOP-elevated (laser-irradiated) eye, because immunostaining of visual cortical sections with an anti-Zif268
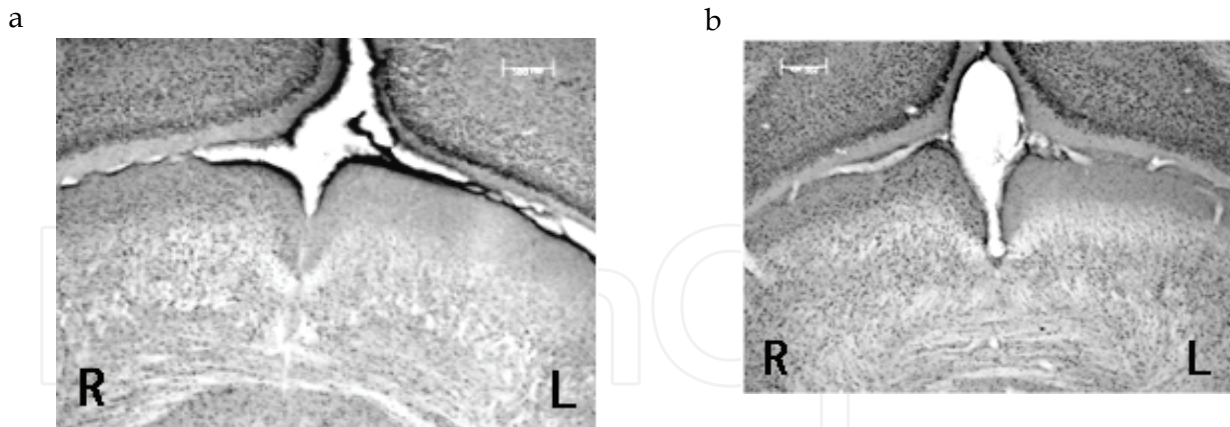
Fig. 9. Immunohistochemical staining of the superior colliculus (SC) of the TTX-injected mouse (a) and enucleated mouse (b) with an anti-zif268 antibody.
The left SC was free of zif268-positive nuclear staining, indicating neuronal activity of the right eye was suppressed by the injection of TTX or the enucleation of eyeball.
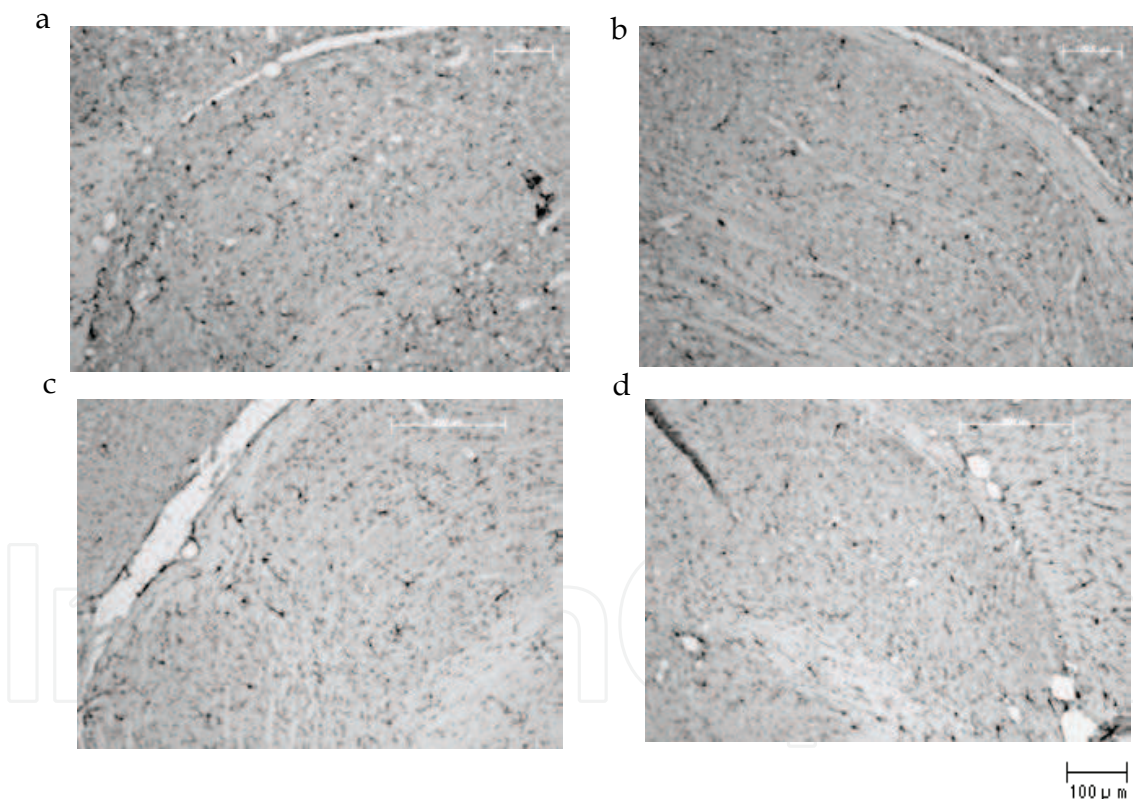


Fig. 10. Iba1 immunostaining of the mouse LGN. Right (a, c) and left (b, d) LGN of the mice, in which their right eye was injected with TTX (a, b) or enucleated (c, d), respectively.

antibody clearly exhibited ocular dominance patches indicating that neuronal activity was suppressed in columns corresponding to the glaucomatous eye (Fig. 11). Under this situation, the microglia are activated in the LGN. This means that maintenance of an adequate level of the retinal activity is critical in keeping the extent of microglia activation low in the central visual pathway.
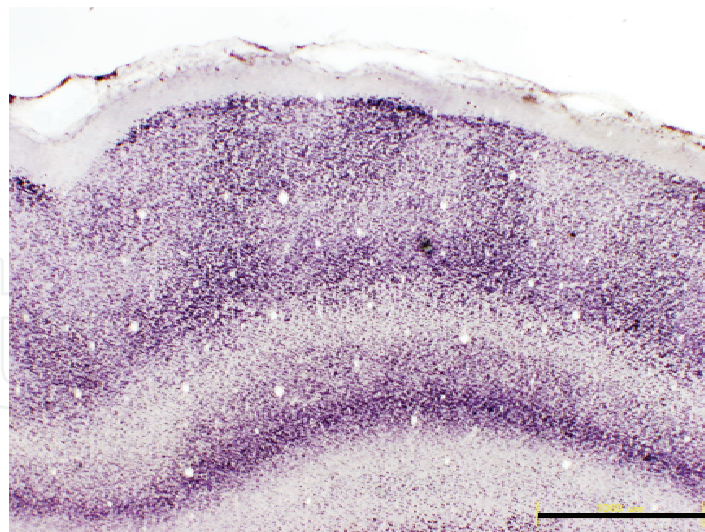
Fig. 11. Ocular dominance patches revealed by zif268 immunohistochemistry of the visual cortex of glaucomatous monkey. Scale, 1.0 mm.

A recent in vivo two-photon imaging study (Wake et al., 2009) reported that resting microglia contact with synapses once an hour and that this contact is neuronal activity-dependent. Intriguingly, transient ischemia prolonged the contact for one hour and presynaptic buttons disappeared after that. These finding is consistent with our findings in the LGN of glaucomatous monkeys.

## 5. Electrophysiological recordings of LGN neurons in monkey with experimentally-induced glaucoma

### 5.1 Background

Single-neuron recording from the primate LGN is useful for studying abnormalities in visual responses in experimental glaucoma (Smith et al., 1993). The primate LGN was selected as a primary site for investigation because of its striking similarities to the human LGN (Spear et al., 1994; O'Keefe et al., 1998) and the response properties of LGN neurons in normal monkeys have been extensively studied (Lee et al., 1979; McClurkin and Marrocco, 1984; Wilson and Forestner, 1995; Usrey and Reid, 2000; Levitt et al., 2001).

Yücel et al. (2000) obtained the following findings for the parvo (P) and magnocelular (M) laminas that receive inputs from the glaucomatous eye: i) there was a significant loss of LGN relay neurons, ii) the loss increased with increase in extent of the RGC loss, iii) neuronal atrophy occurred as measured with decrease in the cross-sectional area of neurons stained with parvalbumin, and iv) the degree of atrophy in the M and P pathways was linearly related to the extent of RGC loss. These are the first findings in the central nervous system that when transsynaptic degeneration occurs, and the extent of target neuron loss in the brain center linearly increases with increasing loss of afferent fibers (Yücel et al., 2001). More specifically, one recent report has engaged our interest by reporting the expansion of visual receptive fields in the SC after the experimental elevation of IOP in one eye (King et al., 2006). They authors suggested that the expansion was induced by enlargement of dendritic field diameter of the retinal ganglion cells due to the elevation of IOP (Ahmed et al., 2001). Thus, along the same line or reasoning, we investigated electrophysiologically the following matters: i) characterization of the neural changes in the LGN of glaucomatous

monkeys, particularly focusing on size changes in minimum response field (MRF) of neurons, ii) to determine whether the extent of such changes differ between the P- and M pathways, and iii) to compare the changes in response properties of LGN neurons between stimulation of glaucomatous and normal eyes.

Three adult male cynomologus monkeys (Macaca fascicularis, GM1-3, Table 1) were used.

| Subject I.D. | Eye | initial IOP mmHg | Age at the 1st LI (postnatal months) | Age at the 2nd LI (postnatal months) | Final IOP mmHg | C/D ratio (HRT) | Age at the start of Physiological Recordings (postnatal months) |
|---|---|---|---|---|---|---|---|
| GM1 | R | - | | | 22.3 | 0.149 | 90 |
| | L | - | 62 | 62 | 46.7 | 0.720 | |
| GM2 | R | 20.5 | | | 14.0 | 0.063 | 61 |
| | L | 18.0 | 54 | 55 | 29.7 | 0.526 | |
| GM3 | R | 16.5 | | | 17.2 | 0.271 | 59 |
| | L | 15.0 | 51 | 51 | 38.7 | 0.740 | |

Table 1. Experimental subjects
IOP, intraocular pressure; LI, laser irradiation; HRT, ophthalmological examination by Heidelberg Retina Tomography; -, no measurement. Data in GM2 and GM3 were cited from 2 monkeys out of 11 previously described in (Shimazawa et al., 2006).

## 5.2 Changes in IOP and funduscopic images of the glaucomatous monkeys

The experimental manipulation and IOP changes that follow over time are summarized for each of the three experimental monkeys in Table 1. In the present study, experimental glaucoma was induced in the left eye. All the three with glaucoma survived for 6 months or longer.

Figure 12 shows the time course of changes in IOP of monkeys GM2 and GM3. Within one month after laser irradiation, the IOP of the treated left eye was significantly elevated and remained high over the following three months. For GM1, however, IOP was measured twice a day (~12 hr apart) only at four different timings. At postnatal month 63, IOPs were $53.3 \pm 2.22$ and 21.0 in glaucomatous and normal eye, respectively. At postnatal month 66, IOPs were still significantly elevated for glaucomatous eye as compared to the normal ($52.6 \pm 2.51$ vs $19.8 \pm 1.28$, $p < 0.0001$, student t-test). There was little variation in IOP measurements within a day.

Figure 13 shows representative funduscopic images obtained from GM2 using HRT. The results of optic disk examinations are summarized in Table 2. The reference plane of HRT was 50 μm deep from the temporal edge of the papilla. The "cup" area and "cup volume are defined, respectively, as a 2D and 3D space deeper below the reference plane. The cup/disk area ratio of the optic disk (C/D ratio) is defined as the average diameter of the cup area divided by that of the disk or the optic nerve head in the retina. The C/D ratio, cup area, volume, and depth were substantially higher in the left eye, which consistently exhibited high IOPs (Table 2). The rim area and rim volume (green and blue areas in Figs. 13 **c** and **d**) reflecting the mean thickness of the nerve fiber lamina, appeared to be smaller in the glaucomatous eye (Fig. 13d). Cupping of the optic papilla was clearly observable in the left eye of the three experimental animals. Albeit the three showed a similar C/D ratios at the time of physiological recording, ophthalmological examinations estimated the severity of their glaucomatous changes as GM1 > 3 > 2 in a decreasing order.
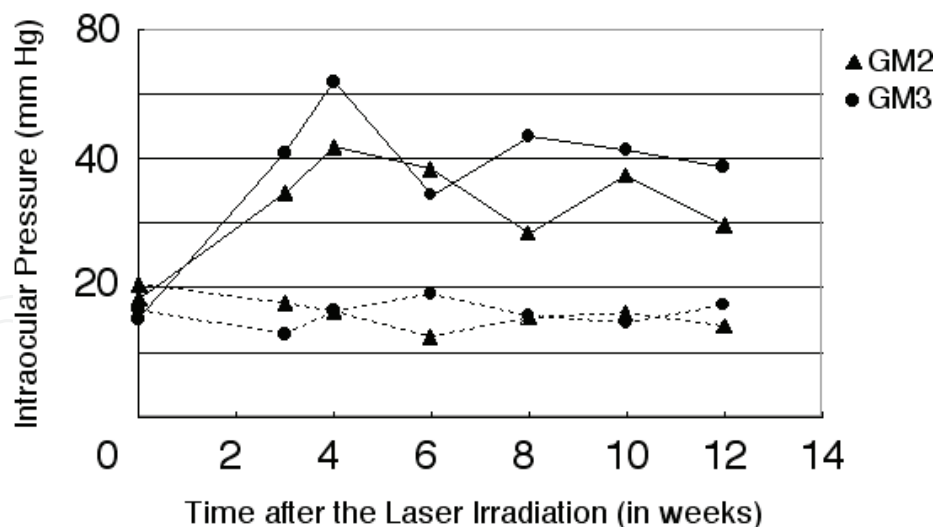
Fig. 12. Time course of changes in IOP (monkey GM2, triangles and GM3, circles) following laser irradiation. Solid lines and dotted lines indicate IOPs of the treated and untreated eyes, respectively. Each data point shows the mean of three measurements. Two measurements were taken within a day (~12 hr apart) on the four different days of examinations to determine the short-term fluctuation in IOP measurements (monkey GM1). Irradiation was performed about one month before the first measurement (i.e. postnatal month 62). At postnatal month 63, IOPs of glaucomatous and normal eyes were $53.3 \pm 2.22$ (mean ± standard deviation) and 21.0 mmHg, respectively. At postnatal month 66, IOPs were still significantly different ($52.6 \pm 2.51$ vs $19.8 \pm 1.28$, $p < 0.0001$, Student t-test). IOPs of GM2 and GM3 were cited from 2 monkeys out of 11 previously described in (Shimazawa et al., 2006).

## 5.3 Impairment of electrophysiological responses

Referencing a brain map of the macaque monkey, lacquer-coated stainless steel electrodes with relatively low impedance (0.5 MΩ at 50 Hz) were initially used to locate the position of the LGN, based on the standard stereotaxic procedure. Then, a glass-coated, high-impedance (>2.0 MΩ at 50 Hz) tungsten microelectrode (Levick, 1972) was introduced into the LGN through a guide cannula vertically placed in the agar-sealed chamber. Action potentials of single neurons were conventionally amplified and monitored on a storage oscilloscope. Minimum response fields (MRFs) (Hubel and Wiesel, 1961; Barlow et al., 1967; Cleland et al., 1983) were routinely mapped with a moving, high contrast light slit and a small spot of flashing light. The border of response fields was repeatedly examined before a circle with an appropriate diameter was respectively assigned to them as authentic MRFs.

The LGN in each cerebral hemisphere represents the nasal hemifield of the contralateral eye, and the temporal hemifield of the ipsilateral eye. The LGN is a thalamic relay structure in the centripetal; projection pathway of the visual system composed of 6 principal laminae of neurons, each of which receives eye-specific inputs: laminae 1, 4, and 6 receive inputs from the contralateral eye, while laminae 2, 3, and 5, input from the ipsilateral eye (Perry et al., 1984). By electrode penetrations that pass vertically through the entire extent of the LGN, it is possible to record from relay neurons of two main types, P- and M neurons, which have receptive fields in approximately corresponding regions of the visual field for the two eyes. Upon the completion of single-neuron recording, we histologically confirmed our assignment of the laminar location to each of many recorded neurons along a given track, using micromanipulator reading during recording.
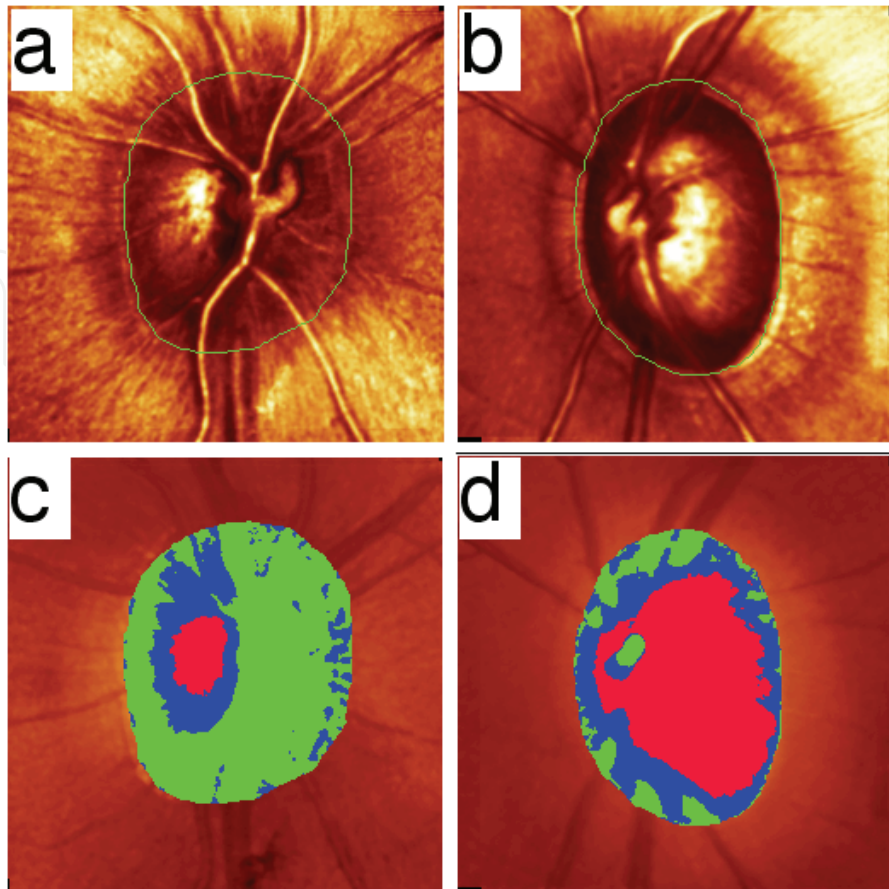
Fig. 13. Representative confocal images (**a** and **b**) of the optic disc and topographic images of HRT (**c** and **d**) in normal (**a** and **c**) and glaucomatous (**b** and **d**) eyes of monkey GM2. Red areas in the optic discs (**c** and **d**) indicate "cupping". Green and Blue areas in **c** and **d** indicate the so-called "rim area", reflecting change in nerve fiber layers (NFL). In the left eye with high IOP, mean NFL thickness was less than in the right eye (0.157 vs. 0.315 mm).

| | GM1 | | GM2 | | GM3 | |
|---|---|---|---|---|---|---|
| | Right | Left | Right | Left | Right | Left |
| Disk Area (mm2) | 1.322 | 1.647 | 1.643 | 1.676 | 1.807 | 1.754 |
| Cup Area (mm2) | 0.198 | 1.182 | 0.103 | 0.882 | 0.49 | 1.297 |
| Cup/Disk Area Ratio | 0.149 | 0.72 | 0.063 | 0.526 | 0.271 | 0.74 |
| Rim Area (mm2) | 1.123 | 0.465 | 1.54 | 0.793 | 1.317 | 0.457 |
| Height Variation Contour (mm) | 0.315 | 0.367 | 0.487 | 0.216 | 0.347 | 0.154 |
| Cup Volume (mm3) | 0.017 | 0.327 | 0.008 | 0.154 | 0.079 | 0.668 |
| Rim Volumn (mm3) | 0.234 | 0.082 | 0.574 | 0.112 | 0.305 | 0.055 |
| Mean Cup Depth (mm) | 0.117 | 0.347 | 0.127 | 0.226 | 0.175 | 0.538 |
| Maxmum Cup Depth (mm) | 0.374 | 0.699 | 0.419 | 0.559 | 0.534 | 0.953 |
| Cup Shape Measure | -0.22 | 0.003 | -0.271 | -0.109 | -0.21 | 0.067 |
| Mean RNFL Thickness | 0.21 | 0.13 | 0.315 | 0.157 | 0.231 | 0.126 |
| RNFL Cross Section Area (mm2) | 0.868 | 0.597 | 1.432 | 0.724 | 1.015 | 0.594 |
| Intraocular Pressure (mmHg) | 22.3 | 46.7 | 14 | 29.7 | 17.2 | 38.7 |

Table 2. Ophthalmological examination by HRT. Data in GM2 and GM3 were cited from 2 monkeys out of 11 previously described in (Shimazawa et al., 2006).
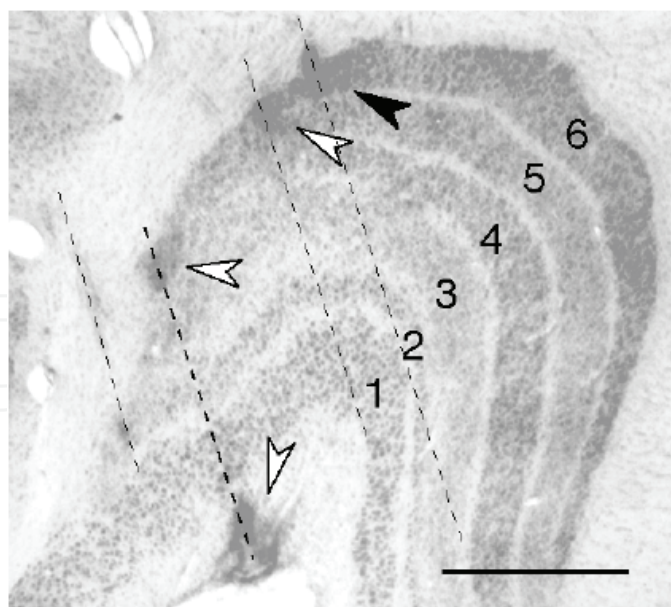
Fig. 14. Histological reconstruction of the recording tracks on Nissl-stained coronal sections obtained from a monkey.
Four arrowheads indicate electrolytic lesions on the recording tracks (dotted lines). The solid arrowhead indicates the location of a neuron whose responses are shown in Fig. 16. Note that the most medial penetration directly entered the magnocellular layers.  The numbers indicate the 6 main laminas of the monkey lateral geniculate nucleus.  Scale bar 1 mm.

Figure 14 shows an example of a photomicrograph of a Nissl-stained coronal section at the middle level of the LGN in the left hemisphere ipsilateral to the glaucomatous eye.  No gross abnormality is noted in Nissl morphology.  We first determined the lamina location of each recorded neuron from the stereotypical shift in eye preference of the receptive fields as our recording electrode was advanced vertically through the different LGN laminas.

Previous studies showed that, up to an eccentricity of 30 degrees, the MRF of LGN neurons in monkey was smaller than three degrees (Schiller et al., 1976; Lee et al., 1979; Bauer et al., 1999; McClurkin et al., 1991; White et al., 2001; Solomon et al., 2002).  Solomon et al. (2002) reported that the classical center radius ($r_c$) of parvo- and magnocellular cells could be estimated by the following equations, respectively:

Parvo:   $r_c = \exp(0.11x - 3.4)$
Magno:  $r_c = \exp(0.07x - 2.4)$
            x, eccentricity (in degree)

Figure 15 shows plots of the MRF of LGN neurons obtained from monkeys GM1 (Fig. 15**a**), GM2 (Fig. 15**c**), and GM3 (Fig. 15**e**) with respective scores for injury found in the head of the optic nerve (Figs. 15**b**, **d**, and **f**). Using more than 10 microelectrode penetrations, we covered the visual field out to ~40 degrees eccentricity in the peripheral visual field.

On stimulation of the normal eye, many small MRFs (each about 1 visual degree across) were found in the peri-foveal region (left plots with a cluster of black circles in Figs. 15**a**, **c**, and **e**). However, no corresponding cluster of small MRFs was found in the central visual field upon stimulation of the glaucomatous eye (right plots with red circles in Fig. 15**a**, **c**, and **e**).  This was particularly clear in monkeys GM1 and GM3, because of the relative lack of spatial overlap of plotted MRFs.
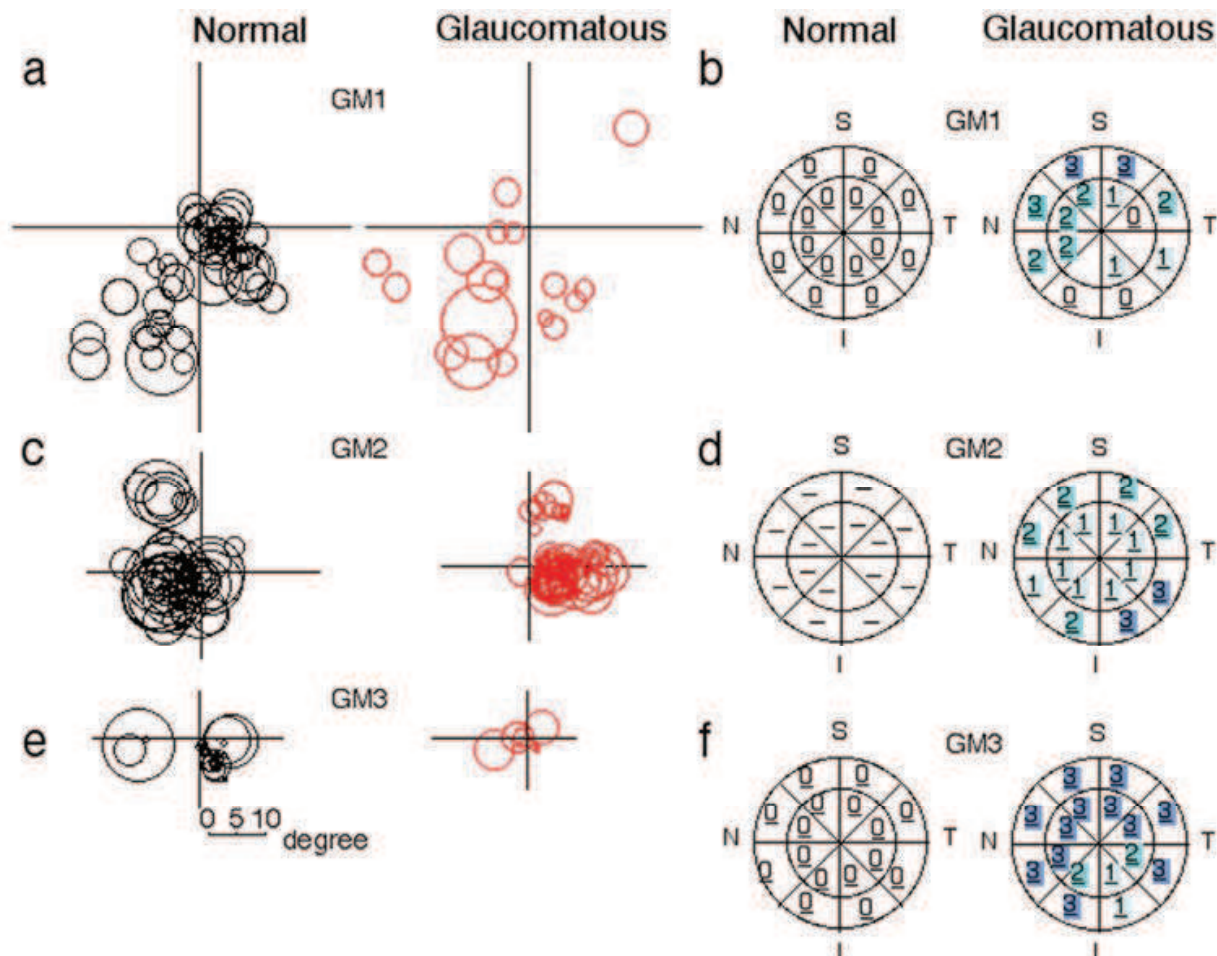
Fig. 15. Plots of the minimum response field (MRF) and diagrams that show injury to the optic nerves in three monkeys (**a** and **b**, monkey GM1; **c** and **d**, monkey GM2; **e** and **f**, monkey GM3).
The MRF of each LGN neurons is rendered as a circle and its boundary indicated by black (normal eye responses, left plots) or red (glaucomatous eye responses, right plots) circles. The horizontal meridian is drawn as a line connecting the two foveas, and the vertical meridian as a line midway between two optic disks. The scale bar shown under the plots for the normal eye of GM3 is common to all MRF plots. Based on the protocol of Sanches et al. (1986), injury to the optic nerve was evaluated histologically (Perry and Cowey, 1985; Wassle et al., 1990; Harwerth et al., 1999). Cross-sections were divided into 16 sectors (8 equal-sized pies, each further halved by an intersecting ring) and the degree of injury in each sector was evaluated microscopically at x 100 with an increasing order of severity: 0, normal; 1, mild (partial atrophy found without hypertrophy of connective tissue); 2, moderate (atrophy of axons with hypertrophy of connective tissue); 3, severe (complete lack of normal axons). S, I, N, and T indicate orientation of the optic nerve head as superior, inferior, nasal, and temporal, respectively.

The pattern and degree of injury to the optic nerve head varied among the three monkeys. Monkeys GM1 and GM3 exhibited more severe injury in the nasal-superior than other sectors, while mild injury was found uniformly in the central sectors of monkey GM3 (Figs. 15**b**, **d**, and **f**). Consistent with this finding, MRFs for the glaucomatous eye were mostly missing from the temporal-inferior visual field of GM1 and GM3.

Intriguingly, we found many extremely large MRFs (>10 degree) in all three monkeys (Figs. 15**a**, **c**, and **e**), suggesting an abnormality in the neural mechanism controlling the size of MRFs in the LGN of glaucomatous monkeys.

### 5.4 Stimulation of glaucomatous and normal eyes

The enlargement of the MRF size of single LGN neurons was observed for both stimulation of normal and glaucomatous eyes (Fig. 15**a**, **c**, and **e**). In the overwhelming majority of 252 recorded neurons, irrespective of which eye was stimulated, the size of MRFs was much larger than one degree across. In GM1, the median MRF size was 4-5 degrees across, while it was 2-3 and 1-2 degrees in GM2 and GM3, respectively (Fig. 16**a-c**). The Wiscoxon signed
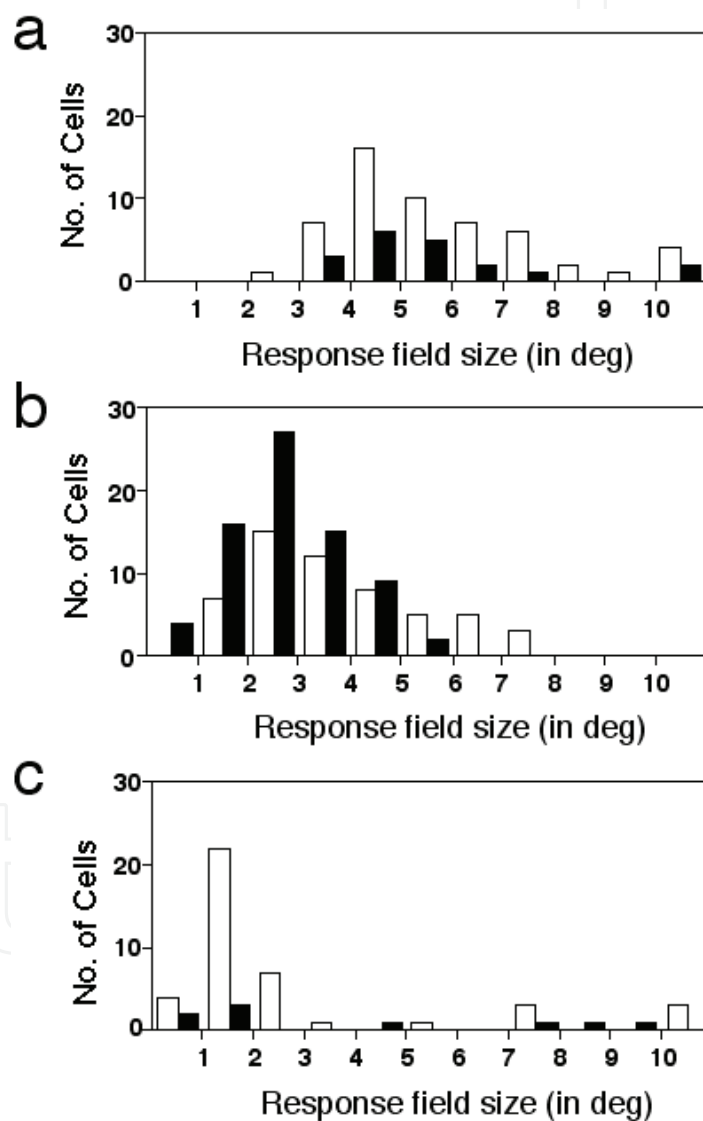


Fig. 16. Frequency histograms of neurons with different MRF sizes in three monkeys (**a**: monkey GM1, **b**: monkey GM2, **c**: monkey GM3).
Filled columns indicate neurons that responded to stimulation of the glaucomatous eye, while open columns indicate those that responded to stimulation of the normal eye. Numbers 2 to 10 on the abscissa indicate size of minimum response field between (n-1) < x ≤ n degrees. Neurons with response field larger than 10 degrees were grouped together as >10.

rank test (using  Prism 4, GraphPad Software Inc., CA U.S.A.) showed that the median derived from the three monkeys was significantly larger in the normal eyes than those in glaucomatous eyes (P<0.037).

Responses to stimulation of the normal eye were more common than to that of the glaucomatous eye in all three monkeys, although the distribution pattern of neurons in the histogram was similar for the two eyes in GM1 and GM2.

Since susceptibility to elevated IOP may differ between different types of RGCs, we suspected the presence of comparable differences in the LGN.  However, we found no marked difference in overall MRF size increase between P and M neurons in the glaucomatous LGN laminas.  This conclusion was based on examination of 170 neurons in P laminas and 73 neurons in M laminas, both of which were included in Fig. 16. We concluded that effects of elevated IOP on MRF size could be obtained in both M- and P-neurons.

### 5.5 Size-tuning curve of LGN neurons

To gain insight into the cellular mechanism underlying the enlargement of LGN receptive fields in glaucomatous monkeys, we investigated their size-tuning properties objectively by stimulating them with a drifting sinusoidal grating patches whose size varied randomly (Akasaki et al., 2002). For the sake of efficiency of the experiments, the application of the objective method was limited to only a part of neurons recorded (N=34) in the above-cited study. Activities of the thus-isolated single neurons were continuously fed to an audio monitor during receptive-field mapping and quantitative data were acquired using a time-stamping board (Lisberger Tech., San Francisco) at a sampling rate of 1 MHz.

Results shown in Figure 17 were obtained from a lamina-6 P neuron whose recording site is shown in Fig. 14 (solid arrow head). Raster plots and PSTHs of the responses to stimuli given to the right normal eye with three different sizes of grating patches are shown in Figs. 17**a**, **b**, and **c**.  The resultant stimulus size-tuning curve is shown in Fig. 17**d**.  This neuron had a MRF of 12.5 degrees.  The response of this neuron was suppressed one time with a patch size of about 21 degrees across (Figs. 17**b** and **d**), but became strong again with increase in patch sizes beyond 28 degrees (Figs. 17**c** and **d**).

Three types of size-tuning behavior were recognized. Two representative size-tuning curves are shown in Figure 18 (**b** and **c)**. First, a neuron with a small MRF exhibited the maximum response at 1.4 degrees, and the response remained strongly suppressed (down to ~ 40% of the maximum) when the patch size was increased beyond this size (Fig. 18**b**). However, having a large MRF of 7.0 degrees, another neuron exemplified in Fig. 18**c** exhibited relatively weak suppression (~73%) with increases in the stimulus patch size beyond 2.1 degrees, which elicited the peak response.  With further increase in stimulus size, the response of this type of cells often became stronger to make a second peak.  The third type exhibited no measurable suppression.

A population of 39 neurons, including 5 not assessed quantitatively, from 7 recording tracks was classified into the three types groups, with about three-quarters of neurons (30 of 39) exhibiting either weak or no suppression at all.

Next, in 34 neurons quantitatively assessed neurons out of the 39 mentioned above, we directly compared the two kinds of size estimates:  one derived from manually plotted MRFs and the other, the receptive field size indices derived from size-tuning curves.  The correlation coefficient (r) was 0.76 and the slope of the fitted line was 1.04, indicating a good correlation between the two measures (Fig. 18**a**, p<0.001).  Most of the points were located
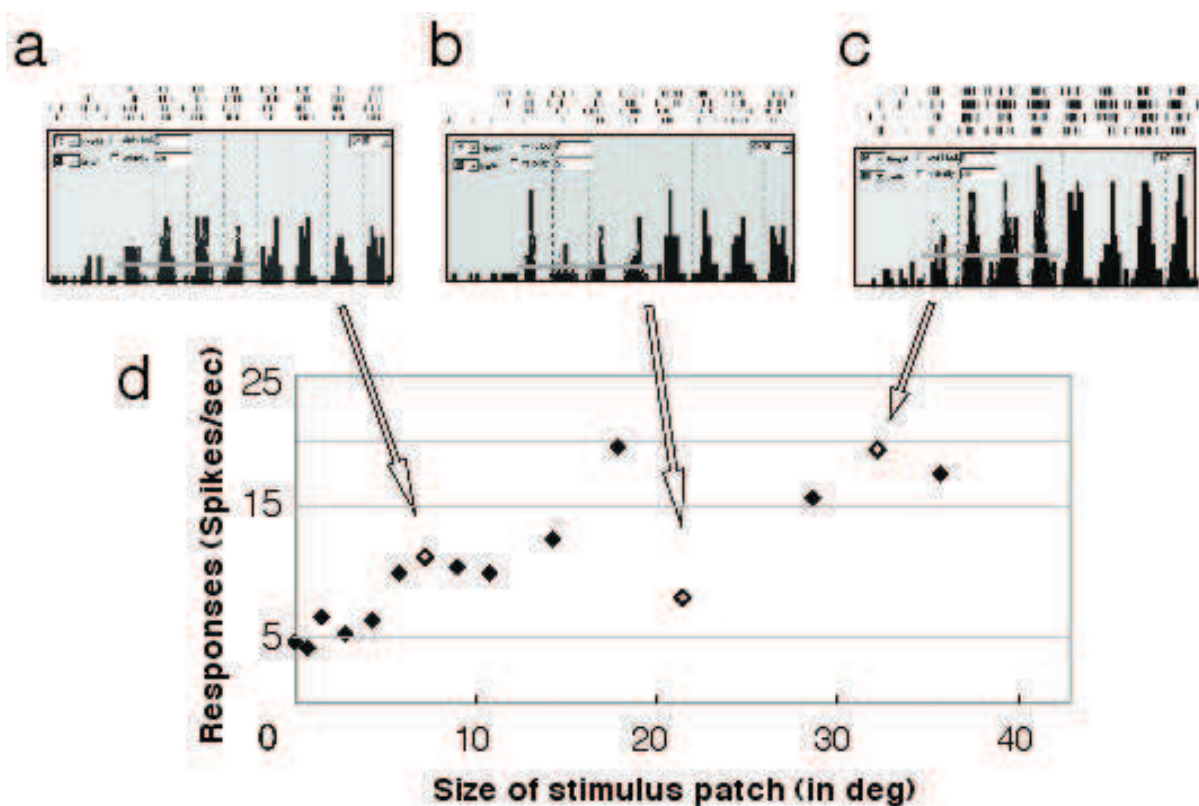
Fig. 17. An example of size-tuning tests.
Three representative peristimulus time histograms (PSTHs) and raster plots (**a**, **b**, **c**) are shown for stimulus sizes indicated by the three open diamonds in **d**. The number of repetition was 6 and bin size was 50 ms for each PSTH. The scale bar under PSTH **c** indicates one sec and is common to **a** and **b**. Mean firing rate (spikes/s) for the first 2 sec after the start of stimulus drift (gray lines in PSTHs) was plotted (filled diamonds) against grating patch size in degrees. The recording site of this neuron is shown in Fig. 14.

above the diagonal dotted line, indicating that the size of MRFs was mostly smaller than the size indices derived from the objective measurements.

In short, the present findings indicate: i) the MRF is usually smaller than the size of the grating patch that evoked the maximum response, while there is a significant correlation between these two measures, and ii) the enlargement of receptive fields of LGN neurons in glaucomatous monkeys was often accompanied by the lack of strong surround suppression. Increase in the cell receptive field size was recently shown in the rat superior colliculus following increase in IOP in one eye (King et al., 2006). The authors suggested that the increase in receptive-field size was related to increase in the size of the dendritic arbors of surviving ganglion cells in the retina. Thus, by the same token, the morphological changes in surviving ganglion cells at the affected eye likely contribute to the emergence of the enlarged receptive fields in the LGN found in the present study.

However, unlike the above-noted findings for rat collicular cells, here in LGN neurons of experimentally induced hypertension glaucomatous monkeys, we found that receptive fields were enlarged with visual stimulation of not only the glaucomatous eye but also the normal eye, which exhibited normal IOP. We suspect that, in the case of LGN neurons, receptive-field enlargement was due to modification of the balance between excitation and
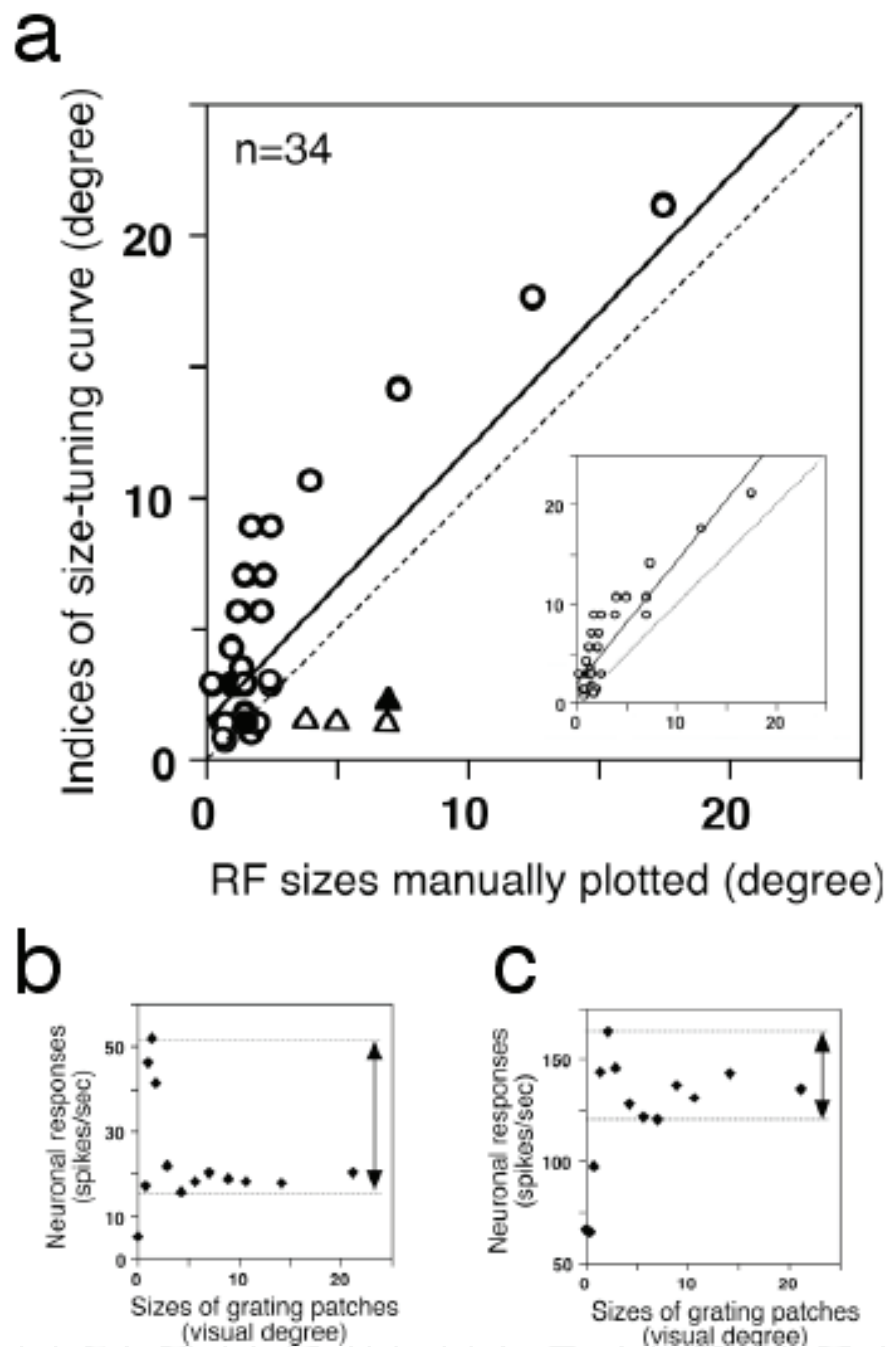
Fig. 18. Correlation between the size of manually plotted MRF and that based on size-tuning curves.

In **a**, the minimum size of the grating patch that evoked the maximum response (peak value or first inflection) was used as a size index for the size-tuning curve. All triangles indicate a group of cells which exhibited a dissociation of these two measures. Size-tuning curves of two representative neurons are shown in **b** (filled square in **a**) and **c** (filled triangle in **a**). In **b** and **c**, the dotted lines with double-headed arrows indicate maximum and minimal responses (i.e. extent of suppression). The solid lines in **a** are fitted by (y=1.04x+1.53) and (y=1.25x+1.87) for the *inset* (triangles excluded), respectively. The dotted lines in **a** are diagonal lines. Data points plotted in **a** appear less than 34 (n=34) because of overlap involving several points.

inhibition. It has been shown that experimental scotoma induces functional reorganization of the primary visual cortex, with enlargement of the receptive fields of neurons representing the region surrounding scotoma into the regions corresponding to scotoma representation (Chino et al., 1992; Gilbert and Wiesel, 1992; Darian-Smith and Gilbert, 1995). When visual stimulation with a discrete patch activates a cluster of thalamic neurons that relay their out put to the cortex, the corresponding feedback projections from the cortex appear to reinforce the core of the thalamic activity by densely focusing on the most active relay neurons while indirectly inhibiting neighboring thalamic neurons in the fringe (Marrocco et al., 1982). This feedback projection narrows the thalamic responsive zone, restricts receptive field sizes, and alters neuronal response properties (Webb et al., 2002). Cortico-thalamic feedback was excitatory when the receptive fields of cortical and thalamic neurons overlapped, but inhibitory when they did not (Tsumoto et al., 1978). Corticofugal feedback also affects the generation of length tuning in the visual pathway: length tuning of LGN neurons was released from cortical control when the visual cortex was cooled (Murphy and Sillito, 1987). In short, the robust effects of corticofugal feedback on geniculate neuron activity suggest that this feedback contributes to the emergence of extremely large MRFs in the LGN in the abnormal conditions.

## 6. Functional implications

The onset of clinical signs is commonly much delayed in glaucomatous patients. Visual abnormality is first noted when injury to the retina has already significantly progressed. In parallel, behavioral measurements in glaucomatous monkeys showed that abnormality in the detection threshold of visual targets was mild despite the severity of injury to the retina (Sasaoka et al., 2005). This suggests the presence of a high level of neural plasticity in the adult brain that compensates for the loss of function due to retinal injury. We found the abnormal enlargement of receptive fields not only with stimulation of the glaucomatous eye but also of the normal eye, suggesting that the mechanism triggering this type of adult plasticity does not reside locally in the retina or even the LGN, but outside of them, probably in visual cortex. This line of reasoning further urges us to study the visual cortex to detect early sign of hypertension glaucoma.

An apparent analogy may be drawn here to the well-known somatosensory field compensation observed in the case of "phantom limbs" (Ramachandran and Rogers-Ramachandran, 2000). In general, the central nervous system readily undergoes reorganization when normal afferents are removed, to compensate for lost function (Wall et al., 1986). Although the basic phenomenology seems to be real in the somatosensory system, in the visual system likelihood of a similar long-term cortical reorganization after retinal lesions is far from settled (Smirmakis et al., 2005). Unlike the acute sensory disturbance induced by cutting or crushing of the optic nerve, in hypertensive glaucoma apoptotic cell death of retinal ganglion cells evolves slowly over a long period of time. The unilateral hypertension model of glaucoma in monkeys thus provides a unique opportunity for not only pathophysiological study on glaucoma ethiology but also study on adult plasticity in the central visual pathways.

## 7. Conclusion

A relatively high incidence of glaucoma has become a serious problem in the modern aging society. In our investigation, we focused on the neural changes along the central visual

pathway in experimentally induced, hypertension glaucoma. First, we used PET in monkeys with unilateral hypertension glaucoma. In 2-[$^{18}$F]fluoro-2-deoxy-glucose studies, monocular visual stimulation of the affected eye yielded significantly reduced neural responses in the occipital areas. The reduction in response was limited to the visual cortex ipsilateral to the affected eye, indicating the unique vulnerability of ipsilateral visual cortex in experimental unilateral glaucoma. Next, in anatomical tracing experiments with WGA, we found in the glaucomatous eye that the retinal projection was selectively damaged in the ipsilateral pathway to the LGN, whereas the contralateral projection was relatively-well preserved. Third, in [$^{11}$C]PK11195 positron emission tomography and immunohistochemical studies, selective accumulation of activated microglia, a sign of neural degeneration, was found bilaterally in the LGN. The accumulation of activated microglia in the LGN is induced plausibly due to the abnormal, either suppressed or enhanced retinal electrical activity. Fourth, in the electrophysiological study on unilateral hypertension glaucomatous monkeys, we found that: i) the existence of "blind" regions in the visual field, in which no receptive field could be found despite multiple penetrations throughout each LGN, ii) the mean size of receptive fields was increased in both glaucomatous-eye-recipient and normal-eye-recipient LGN laminae, iii) the size was significantly larger for the normal-eye than those for glaucomatous eye. In glaucomatous monkeys, receptive field properties of responsive LGN neurons often exhibited little modification except in the receptive-field size. This form of adult plasticity may play a role in neuronal compensation in the central visual pathway of retinal input due to glaucoma. In addition to reduce the ganglion cell death, it is suggested that the enhancement of neural plasticity in the central visual pathway is also important for the remedy of glaucoma. In short, the current findings in experimental hypertension glaucoma seem to support our basic premise that the neural changes along the central visual pathway in glaucoma may precede those in the eye, against the backgroung of the former's high degree of compensation for the deteriorating function.

## 8. Acknowledgements

## 9. References

Ahmed F.A.K.M., Chaudhary, P., & Sharma, S.C. (2001). Effects of increased intraocular pressure on rat retinal ganglion cells. *Int. J. Devl. Neurosci.*, 19, pp. (209-218)

Akasaki, T., Sato, H., Yoshimura, Y., Ozeki, H., & Shimegi, S. (2002). Suppressive effects of receptive field surround on neuronal activity in the cat primary visual cortex. *Neurosci. Res.*, 43, pp. (207-220)

Asano, E., Mochizuki, K., Sawada, A., Nagasaka, E., Kondo, Y., & Yamamoto T. (2007). Decreased nasal-temporal asymmetry of the second-order kernel response of

mulitifocal electroretinograms in eyes with normal-tension glaucoma. *Jpn. J. Ophthalmol.*, 51, 5, pp. (379-389)

Barlow, H.B., Blakemore, C., & Pettigrew, J.D. (1967). The neural mechanism of binocular depth discrimination. *J. Physiol.*, 193 pp. (327-342)

Bauer, U., Scholz, M., Levitt, J.B., Obermayer, K., & Lund, J.S. (1999). A model for the depth-dependence of receptive field size and contrast sensitivity of cells in layer 4C of macaque striate cortex. *Vision Res.*, 39, pp. (613-629)

Cagnin, A, Brooks D.J., Kennedy A.M., Gunn R.N., Myers, R., Turkheimer F.E., Jones, T., & Banati, R.B. (2001a). In-vivo measurement of activated microglia in dementia. *Lancet*, 358, pp. (9280)

Cagnin, A., Myers, R., Gunn, R.N., Lawrence, A.D., Stevens, T., Kreutzberg, G.W., Jones, T., Banati, R.B. (2001b). In vivo visualization of activated glia by [$^{11}$C] (R)-PK11195-PET following herpes encephalitis reveals projected neuronal damage beyond the primary focal lesion. *Brain*, 124, 10, pp. (2014-2017)

Chino, Y.M., Kaas, J.H., Smith, E.L., 3rd, Langston, A.L., & Cheng, H. (1992). Rapid reorganization of cortical maps in adult cats following restricted deafferentation in retina. *Vision Res.*, 32, pp. (789-796)

Cleland, B.G., Lee, B.B., & Vidyasagar, T.R. (1983). Response of neurons in the cat's lateral geniculate nucleus to moving bars of different length. *J. Neurosci.*, 3, pp. (108-116)

Darian-Smith, C., & Gilbert, C.D. (1995). Topographic reorganization in the striate cortex of the adult cat and monkey is cortically mediated. *J. Neurosci.*, 15 pp. (1631-1647)

Elolia, R., & Stokes, J. (1998). Monograph series on aging-related diseases: XI. Glaucoma. *Chronic Dis. Can.*, 19, pp. (157-169)

Fischer, B., & Kruger, J. (1974). The shift-effect in the cat's lateral geniculate neurons. *Exp. Brain Res.*, 21, pp. (225-227)

Fitzgibbon, T., & Taylor, S.F. (1996). Retinotopy of the human retinal nerve fibre layer and optic nerve head. *J. Comp. neurol.*, 375, 2, pp. (238-251)

Gilbert, C.D., & Wiesel, T.N. (1992). Receptive field dynamics in adult primary visual cortex. *Nature*, 356, pp. (150-152)

Giovacchini, G., Squitieri, F., Esmaelizadeh, M, Milano, A., Mansi, L., & Clarmiello A. (2011). PET translates neurophysiology into images: A review to stimulate a network between neuroimaging and basic research. *J. Cell Physiol.*, 226 4, pp. (948-961)

Gong, S, & LeDoux, M.S. (2003). Immunohistochemical detection of wheat germ agglutinin-horseradish peroxisase (WGA-HRP). *J. Neurosci. Methods*, 26, 1, pp. (25-34)

Graeber, M.B., Bise, K., & Mehraein, P. (1994). CR3/43, a merker for activated human microglia: application to diagnostic neuropathology. *Neurophathol. Appl. Neurobiol.*, 20, 4, pp. (406-408)

Harwerth, R.S., Carter-Dawson, L., Shen, F., Smith, E.L., 3rd, & Crawford, M.L. (1999). Ganglion cell losses underlying visual field defects from experimental glaucoma. *Invest. Ophthalmol. Vis. Sci.*, 40, pp. (2242-2250)

Hubel, D.H., & Wiesel, T.N. (1961). Integrative action in the cat's lateral geniculate body. *J. Physiol.*, 155, pp. (385-398)

Imamura, K., Richter, H., Fischer, H. Lennerstrand, G., Franzén, Rydberg, A., Andersson, J., Schneider, H., Onoe, H., Watanabe, Y., & Långström, B. (1997). Reduced activity in the extrastriate visual cortex of individuals with strabismic amblyopia. *Neuroscience Lett.*, 225, pp. (173-176)

Imamura, K., Onoe, H., Shimazawaa, M., Nozaki, S., Wada, Y., Kato, K., Nakajima, H., Mizuma, H., Onoe, K., Taniguchi, T., Sasaoka, M., Hara, H., Tanaka, S, Araie, M., & Watanabe, W. (2009). Molecular imaging reveals unique degenerative changes in experimental glaucoma. *NeuroReport*, 20, pp. (139-144)

King, W.M., Sarup, V., Sauve, Y., Moreland, C.M., Carpenter, D.O., & Sharma, S.C. (2006). Expansion of visual receptive fields in experimental glaucoma. *Vis. Neurosci.*, 23, pp. (137-142)

Klein, B.E., Klein, R., & Linton, K.L. (1992). Intraocular pressure in an American community. The Beaver Dam Eye Study. *Invest. Ophthalmol. Vis. Sci.*, 33, pp. (2224-2228)

Lee, B.B., Creutzfeldt, O.D., & Elepfandt, A. (1979). The responses of magno- and parvocellular cells of the monkey's lateral geniculate body to moving stimuli. *Exp. Brain Res.*, 35, pp. (547-557)

Leske, M.C. (1983). The epidemiology of open-angle glaucoma: a review. *Am. J. Epidemiol.*, 118, pp. (166-191)

Levick, W.R. (1972). Another tungsten micro-electrode. *Med. Biol. Eng.*, 10, pp. (510-515)

Levitt, J.B., Schumer, R.A., Sherman, S.M., Spear, P.D., & Movshon, J.A. (2001). Visual response properties of neurons in the LGN of normally reared and visually deprived macaque monkeys. *J. Neurophysiol.*, 85, pp. (2111-2129)

Marrocco, R.T., McClurkin, J.W., & Young, R.A. (1982). Modulation of lateral geniculate nucleus cell responsiveness by visual activation of the corticogeniculate pathway. *J. Neurosci.*, 2, pp. (256-263)

McClurkin, J.W., & Marrocco, R.T. (1984). Visual cortical input alters spatial tuning in monkey lateral geniculate nucleus cells. *J. Physiol.*, 348, pp. (135-152)

McClurkin, J.W., Gawne, T.J., Richmond, B.J., Optican, L.M., & Robinson, D.L. (1991) Lateral geniculate neurons in behaving primates. I. Responses to two-dimensional stimuli. *J. Neurophysiol.*, 66, pp. (777-793)

Murphy, P.C., & Sillito, A.M. (1987). Corticofugal feedback influences the generation of length tuning in the visual pathway. *Nature*, 329, pp. (727-729)

O'Keefe, L.P., Levitt, J.B., Kiper, D.C., Shapley, R.M., & Movshon, J.A. (1998). Functional organization of owl monkey lateral geniculate nucleus and visual cortex. *J. Neurophysiol.*, 80, pp. (594-609)

Perry, V.H., & Cowey, A. (1985). The ganglion cell and cone distributions in the monkey's retina: implications for central magnification factors. *Vision Res.*, 25, pp. (1795-1810)

Perry, V.H., Oehler, R., & Cowey, A. (1984). Retinal ganglion cells that project to the dorsal lateral geniculate nucleus in the macaque monkey. *Neurosci.*, 12, pp. (1101-1123)

Ramachandran, V.S., & Rogers-Ramachandran, D. (2000). Phantom limbs and neural plasticity. *Arch. Neurol.*, 57, pp. (317-320)

Salive, M.E., Guralnik, J., Christen, W., Glynn, R.J., Colsher, P., & Ostfeld, A.M. (1992). Functional blindness and visual impairment in older adults from three communities. *Ophthalmology*, 99, pp. (1840-1847)

Sanchez, R.M., Dunkelberger, G.R., & Quigley, H.A. (1986). The number and diameter distribution of axons in the monkey optic nerve. *Invest. Ophthalmol. Vis. Sci.*, 27, pp. (1342-1350)

Sasaoka, M., Hara, H., & Nakamura, K. (2005). Comparison between monkey and human visual fields using a personal computer system. *Behav. Brain Res.*, 161, pp. (18-30)

Schiller, P.H., Finlay, B.L., & Volman, S.F. (1976). Quantitative studies of single-cell properties in monkey striate cortex. I. Spatiotemporal organization of receptive fields. *J. Neurophysiol.*, 39, pp. (1288-1319)

Shimazawa, M., Taniguchi, T., Sasaoka, M., & Hara, H. (2006a). Nerve fiber layer measurement using scanning laser polarimetry with fixed corneal compensator in normal cynomolgus monkey eyes. *Ophthalmic Res.*, 38, pp. (1-7)

Shimazawa, M., Tomita, G., Taniguchi, T., Sasaoka, M., Hara, H., Kitazawa, Y., & Araie, M. (2006b). Morphometric evaluation of changes with time in optic disc structure and thickness of retinal nerve fibre layer in chronic ocular hypertensive monkeys. *Exp. Eye Res.*, 82, pp. (427-440)

Smith, E.L,, 3rd, Chino, Y. M., Harwerth, R. S., Ridder, W. H., 3rd, Crawford, M.L.J., & DeSantis, L. (1993). Retinal inputs to the monkey's lateral geniculate nucleus in experimental glaucoma. *Clinical Vision Sci.*, 8, pp. (113-139)

Smirnakis, S.M., Brewer, A.A., Schmid, M.C., Tolias, A.S., Schuz, A., Augath, M., Inhoffen, W., Wandell, B.A., & Logothetis, N.K. (2005). Lack of long-term cortical reorganization after macaque retinal lesions. *Nature*, 435, pp. (300-307)

Solomon, S.G., White, A.J., & Martin, P.R. (2002). Extraclassical receptive field properties of parvocellular, magnocellular, and koniocellular cells in the primate lateral geniculate nucleus. *J. Neurosci.*, 22, pp. (338-349)

Spear, P.D., Moore, R.J., Kim, C.B., Xue, J.T., & Tumosa, N. (1994). Effects of aging on the primate visual system: spatial and temporal processing by lateral geniculate neurons in young adult and old rhesus monkeys. *J. Neurophysiol.*, 72, pp. (402-420)

Tsumoto, T., Creutzfeldt, O.D., & Legendy, C.R. (1978). Functional organization of the corticofugal system from visual cortex to lateral geniculate nucleus in the cat (with an appendix on geniculo-cortical mono-synaptic connections). *Exp. Brain Res.*, 32, pp. (345-364)

Usrey, W.M., & Reid, R.C. (2000). Visual physiology of the lateral geniculate nucleus in two species of new world monkey: Saimiri sciureus and Aotus trivirgatis. *J. Physiol.*, 523, 3, pp. (755-769)

Vowinckel, E., Reutens, D., Becher B., Evans, A., Owens, T., & Antel J.P. (1997). PK11195 binding to the peripheral benzodiazepine receptor as a marker of microglia activation in multiple sclerosis and experimental autoimmune encephalomyelitis. *J. Neurosci. Res.*, 50, 2, pp. (345-353)

Wake, H., Moorhouse, A.J., Jinno, S., Kohsaka S., & Nabekura, J. (2009). Resting microglia directly monitor the functional state of synapses in vivo and determine the fate of ischemic terminals. *J. Neurosci.*, 29, 13, pp. (3974-3980)

Wall, J.T., Kaas, J.H., Sur, M., Nelson, R.J., Felleman, D.J., & Merzenich, M.M. (1986). Functional reorganization in somatosensory cortical areas 3b and 1 of adult monkeys after median nerve repair: possible relationships to sensory recovery in humans. *J. Neurosci.*, 6, pp. (218-233)

Wassle, H., Grunert, U., Rohrenbeck, J., & Boycott, B.B. (1990). Retinal ganglion cell density and cortical magnification factor in the primate. *Vision Res.*, 30, pp. (1897-1911)

Webb, B.S., Tinsley, C.J., Barraclough, N.E., Easton, A., Parker, A., & Derrington, A.M. (2002). Feedback from V1 and inhibition from beyond the classical receptive field modulates the responses of neurons in the primate lateral geniculate nucleus. *Vis. Neurosci.*, 19, pp. (583-592)

White, A.J., Solomon, S.G., & Martin, P.R. (2001). Spatial properties of koniocellular cells in the lateral geniculate nucleus of the marmoset Callithrix jacchus. *J. Physiol.*, 533, pp. (519-535)

Wilson, J.R., & Forestner, D.M. (1995). Synaptic inputs to single neurons in the lateral geniculate nuclei of normal and monocularly deprived squirrel monkeys. *J. Comp. Neurol.*, 362, pp. (468-488)

Yücel, Y.H., Zhang, Q., Gupta, N., Kaufman, P.L., & Weinreb, R.N. (2000). Loss of neurons in magnocellular and parvocellular layers of the lateral geniculate nucleus in glaucoma. *Arch. Ophthalmol.*, 118, pp. (378-384)

Yücel, Y.H., Zhang, Q., Weinreb, R.N., Kaufman, P.L., & Gupta, N. (2001). Atrophy of relay neurons in magno- and parvocellular layers in the lateral geniculate nucleus in experimental glaucoma. *Invest. Ophthalmol. Vis. Sci.*, 42, pp. (3216-3222)
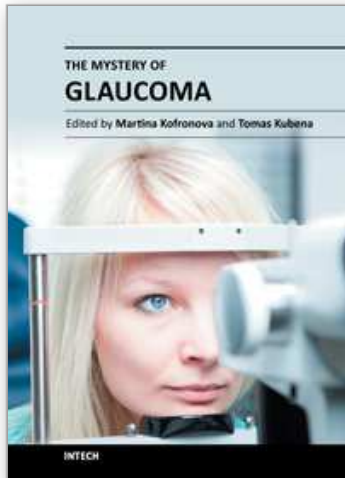
**The Mystery of Glaucoma**

Edited by Dr. Tomas Kubena

Since long ago scientists have been trying hard to show up the core of glaucoma. To its understanding we needed to penetrate gradually to its molecular level. The newest pieces of knowledge about the molecular biology of glaucoma are presented in the first section. The second section deals with the clinical problems of glaucoma. Ophthalmologists and other medical staff may find here more important understandings for doing their work. What would our investigation be for, if not owing to the people's benefit? The third section is full of new perspectives on glaucoma. After all, everybody believes and relies – more or less – on bits of hopes of a better future. Just let us engage in the mystery of glaucoma, to learn how to cure it even to prevent suffering from it. Each information in this book is an item of great importance as a precious stone behind which genuine, through and honest piece of work should be observed.

# INTECH
open science | open minds